1/f frequency noise in a communication receiver and the Riemann hypothesis

Michel Planat

Laboratoire de Physique et Métrologie des Oscillateurs du CNRS, 32 Avenue de l'Observatoire, 25044 Besançon Cedex, France

Abstract. A mixer cascaded with a low pass filter is the basic piece of any communication receiver. It is also used to register minute frequency fluctuations of an external oscillator (RF) under test versus the frequency of a local oscillator (LO). Such a scheme may also be viewed as the basic model of an electronic oscillator, with the amplifier noise at the RF input and the resonator signal at the LO input. We have investigated experimentally the whole spectrum of frequencies and amplitudes of beat signals and their frequency fluctuations at the IF output of the mixer + filter set-up. We have found evidence that all the dynamics follows arithmetical rules. As for the frequency of the beat signal it is defined from a diophantine approximation of the frequency ratio of input oscillators. As for the amplitude it is defined globally from the position of resolved fractions with respect to the equally spaced graduation. As for the frequency fluctuations a transition from white frequency noise to 1/f frequency noise is observed close to resonance. It is explained on the basis of number theory in relation to the Riemann problem concerning the distribution of prime numbers. More precisely it is shown that diophantine signal processing is at work in the receiver and that may be understood from the Littlewood and Franel-Landau formulation of the Riemann hypothesis.

1 The communication receiver

1.1 Theoretical background

Although it may have a quite complex architecture, the basic piece of a communication receiver is close to the one proposed by Amstrong for broadcast reception. That technique revives today in wireless applications. The receiver is designed to compare the information carying external oscillator (called RF) to a local oscillator (called LO) of about the same high frequency through a nonlinear mixing element. For narrow band FM demodulation (which is typical for broadcasting and wireless analogic applications) one uses a discriminator of which the role is first to differentiate the signal, that is convert frequency modulation (FM) to amplitude modulation (AM) and second to detect its low frequency envelope: this is called baseband filtering. For more general wideband or narrowband FM demodulation one uses a low frequency filter instead of the discriminator to remove the high frequency signals generated after the mixer.

In the closed loop operation a voltage controlled LO is used to track the frequency of the RF (hence the generic words: FMFB for a FM feedback loop or PLL for a phase locked loop). Phase modulation is becoming most frequently used for digital signals because low bit error rates can be obtained for relatively poor signal to noise ratio, in comparison to frequency modulation [1].

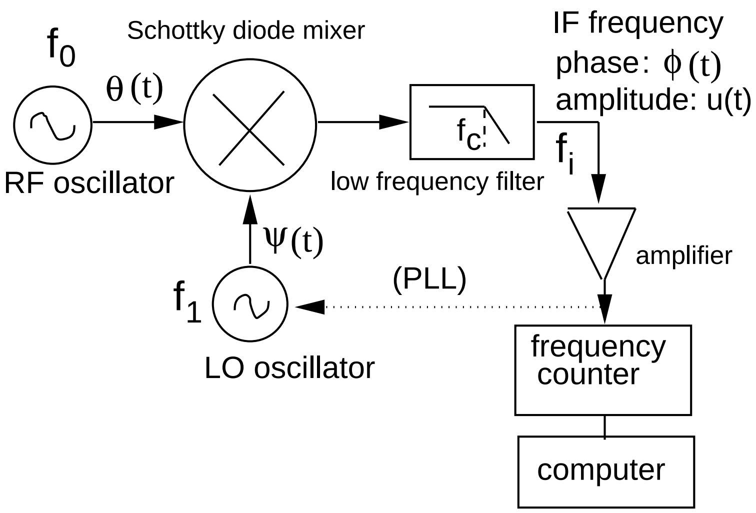

Fig. 1. Schematic of the electronic set-up used in the experiment

In this paper we will consider that the basic piece of the receiver includes a multiplier (or mixer) cascaded with a lowpass filter (in the closed loop operation, this is the PLL). Such a set up (Fig. 1) is widely used in frequency metrology to register minute frequency fluctuations of an external RF oscillator under test versus the frequency of a local LO oscillator. Mixing operation results from the frequency conversion in the time varying conductance of the diode, or the transconductance from gate to drain in a field effect transistor. Here we use Schottky barrier diodes in a doubly balanced structure to produce good isolation between the inputs [2].

The ideal mixer multiplies the RF signal of frequency f_o to be received by the reference sinusoid of frequency f_1 of the LO shifting in both to the sum frequency and the difference frequency $f_0 \pm f_1$. The down conversion at the intermediate frequency (called IF) is desired so that a low pass filter of cut-off frequency f_c is included. In such a configuration the set mixer + filter essentially behaves as a phase detector, that is the instantaneous voltage at the output is the sine of the phase difference at the inputs:

$$u(t) = a\ sin(\theta(t) - \psi(t)) \tag{1}$$

where $\theta(t)$ and $\psi(t)$ are the instantaneous phases of the RF and LO oscillators and a (in Volts per radian) is the phase detector sensitivity. The non linear dynamics of the set-up in the closed loop configuration is well described by introducing the phase difference $\phi(t) = \theta(t) - \psi(t)$. Using $\dot{\theta} = \omega_0$ and $\dot{\psi}(t) = \omega_1 + A\ u(t)$ with $\omega_0 = 2\pi\ f_0$, $\omega_1 = 2\pi\ f_1$ and A (in rad. Hz/Volt) the sensitivity of the voltage controlled oscillator (called VCO) one obtains the non linear differential eq.

$$\dot{\phi}(t) + K\ sin(\phi(t)) = \omega_i \tag{2}$$

with $\omega_i = \omega_0 - \omega_1$ as the bare frequency shift between the input oscillators and the frequency $K = aA$ as the coupling coefficient (also called open loop gain). Eq. (2) is integrable but its solution looks complex [4]. If the frequency shift ω_i does not exceed the open loop gain K, the average frequency$\langle\dot{\phi}\rangle$ vanishes after a finite time to reach the stable steady state $\phi(\infty) = 2l\pi + sin^{-1}(\omega_i/K)$, l integer. In this phase tracking range of width $2K$ the RF and LO oscillators are also frequency locked. Outside the modelocking zone there is a sech shape beat signal of frequency

$$\omega_B = \langle\dot{\phi}(t)\rangle = K(u^2-1)^{1/2}\ that\ is\ \omega_B = (\omega_i^2 - K^2)^{1/2}, \tag{3}$$

with $u = \omega_i/K$ converging to the open loop frequency ω_i as $u << 1$.

Due to the nonlinearity of the mixer the practical operation of the phase detector also involves the harmonic interactions

$$u(t) = \sum_{p,q} a^{(p,q)}\ sin(q\theta(t) - p\psi(t)) \tag{4}$$

leading to the intermodulation frequencies

$$f_i^{(p,q)} = \mid pf_0 - qf_1 \mid \ \ with\ p\ and\ q\ integers \tag{5}$$

in the bandwidth of the filter [4]. Standard models account for non linear interactions resulting from the LO excitation only, assuming the RF excitation is negligible. We found in section 2 an alternative way of thinking the spectrum of frequency mixings based on number theory and specifically on continued fraction expansions (CFE) of frequency ratios of signals at the input of the mixer.

From this form we can expect the device will produce a rational approximation of the frequency ratio $\nu = f_1/f_0$. We will show below that it behaves as a diophantine approximator. This is in contradiction with the conventional view of filtering that we remind from now. In such a linear approach the loop filter is represented from the Laplace transform $H_2(P)(P = \frac{d}{dt}) = .$ so that instead of eq. (1) we get

$$u(t) = a\ H_2(P)\ sin\ \phi(t) \tag{6}$$

and the nonlinear dynamics is described from

$$\dot{\phi}(t) + K\ H_2(P)\ sin\ \phi(t) = \omega_i \tag{7}$$

The loop filter is typically a low pass filter of overall transfer function

$$H_2(P) = \frac{1 + \frac{P}{A}}{1 + \frac{P}{B}} \tag{8}$$

leading to the describing equation

$$\ddot{\phi}(t) + \dot{\phi}(t)(B + KB/A\ cos\phi(t)) + BK\ sin\phi(t) = B\omega_i \tag{9}$$

The linear description of the PLL leads to the closed loop transfer function [1]

$$H(P) = \frac{1 + \frac{P}{a_0\omega_n}}{(\frac{P}{\omega_n})^2 + 2\eta\frac{P}{\omega_n} + 1} \tag{10}$$

with $\omega_n = (KB)^{1/2}$, $\eta = 1/2(B/K)^{1/2} + (KB)^{1/2}/2A$ and $a_0 = A/(K)B^{1/2}$. This closed loop transfer function is similar to the one in a FMFB loop. There is a complex pole pair of natural frequency ω_n, a damping factor η and a real zero at $P = -a_0\omega_n$.

The non linear operation is much more complicated allowing for the so-called cycle skipping phenomenon, i.e. the trajectory in phase space may leave the main attractive region through successive cycles of 2π phase error. This beat signal looks similar to the one described in eq. (3) when the initial frequency offset is outside the phase-locked range K. As shown below we found experimentally a 1/f frequency spectrum associated to that phenomenon [4]. It represents one of the main motivations for the arithmetical approach.

A full understanding of the cycle skipping phenomenon and the associated 1/f frequency spectrum needs an account of the intermodulation products which are present at the output of the receiver. Using eq. (4) instead of eq. (1), the PLL eq. (7) is generalized as:

$$\dot{\phi}^{(p,q)}(t) + q\ H_2(P) \sum_{r,s} K^{(r,s)} sin\ \phi^{(r,s)} = \omega_i^{(p,q)} \tag{11}$$

where $\omega_i^{(p,q)} = p\omega_0 - q\omega_1$, and $K(r,s)$ is the effective gain at the harmonic (r,s) and $H_2(P)$ is the open loop gain as in eq. (8).

Eq. (11) can be rewritten for two individual modes (p,q) and (m,n) and the sum over (r,s) removed. After integration we obtain:

$$\dot{\phi}^{(p,q)}(t) + q\ H_2(P) \sum_{r,s} K^{(r,s)} sin(\frac{s}{q}\ \phi^{(p,q)} - \frac{\omega_0 t}{q}(qr - ps) + \phi_0^{(r,s)}) = \omega_i^{(p,q)} \tag{12}$$

where $\phi_0^{(r,s)}$ is a reference phase at harmonic (r,s). We didn't undertake the task to study the differential eq. (12) in detail because the arithmetical approach below will be far more efficient. However some hints concerning the non linear interactions are given now. Let us first consider the case of a first order filter $H_2(P) = 1$. If one neglects the interaction of one product with the other so that $\frac{p}{q} = \frac{r}{s}$, one recovers an eq. similar to (7) at each harmonic. In the general case it is observed from (12) that the RF signal acts as periodic perturbation for the standard PLL loop. In order to illustrate the net effect of introducing such perturbations, we consider the realistic case of the interaction of the fundamental $(p, q) = (1, 1)$ with the main odd subharmonic at $(r, s) = (1, 3)$. In such a case eq. (12) simplifies as:

$$\dot{\phi(t)} + K\ sin(\phi(t)) + K^{(3)} sin(3\phi(t) + 2\omega_0 t) = \omega_i \tag{13}$$

where we used $\phi = \phi^{(1,1)}$ and $K = K^{(1,1)}$ and $K^{(3)} = K^{(1,3)}$. In ref. [3] we described an asymptotic perturbation analysis for deriving mode-locked zones in eq. (13). If the condition $\dot{\phi(t)} = C^{te}$ holds over each cycle provided the counting time is large enough in comparison to the period, we can get a recurrence formula mapping the phase ϕ_{n+1} at time $t + 2\pi/\omega_0$ to that ϕ_n at time t with the following form:

$$\phi_{n+1} = \phi_n + 2\pi\omega - c\ sin\phi_n - d\ sin(3\phi_n) \tag{14}$$

with $\omega = \omega_i/\omega_0$, $c = 2\pi K/\omega_0$ and $d = 2\pi K^{(3)}/\omega_0$. Eq. (14) extends the well known Arnold map.

Such an eq. is studied by introducing the winding number The curve ν_{av} versus ω is a devil's staircase with steps attached to rational values of $\omega = p/q$ and their width increasing with the coupling coefficient c. In ref. [5] we presented an approach to plot the mode-locked zones (called Arnold tongues) based on the introduction of an Hölder exponent. In the present case $d << c << 1$ so that we stay very far from the critical value c=1 where the tongues may recover and chaotic states may be present. This means that the cycle skipping phenomenon and the 1/f frequency noise are not related to the type of chaos predicted from the Arnold map. If we turn to the second order filtering effect in eq. (8), we get instead of (14) a two dimensional map extending the well known standard map [6].

1.2 Experiments

We derived above a non linear differential model, eq. (12) taking into account the full intermodulation spectrum at the output of the demodulator. We now present the experimental motivation for that work and the reasons why it should be further improved to get a full consideration of the frequency and amplitude spectra and of the associated frequency fluctuations. All the experiments below are given for the PLL in the open loop configuration. They can be regarded as an asymptotic low coupling limit for eq. (12). We used a $f_0 = 10\ MHz$ RF oscillator and a LO oscillator of frequency varying from $f_1 = 100\ kHz$ up to $f_1 = 10\ MHz$, interacting through a wideband doubly balanced Schottky diode mixer (Fig. 1). The low frequency filter can be approximated to a second order type one with $f_n \sim \omega_n/2\pi = 375\ kHz$. It is observed in fig. 2 that there are many subharmonic modes $\nu = p/q$ in addition to the fundamental one at $\nu = 1/1$. The main ones correspond to p and q odd; intermodulation products at p or q even are strongly rejected due to the doubly balanced phase bridge structure of the mixer. Each mode is resonant and extends over a basin which is controlled from the low frequency cut off of the loop filter, the full dynamics of the subharmonics and the thermal noise of the input oscillators. In order to get valuable insights into

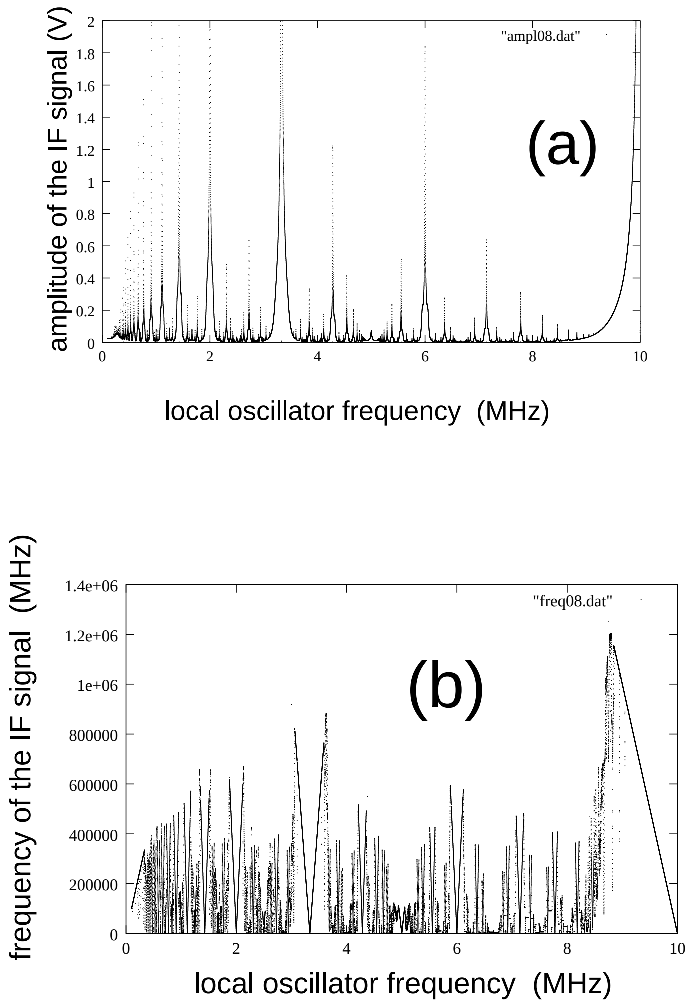

Fig. 2. The amplitude spectrum (top) and the frequency spectrum (bottom)

these seemingly complicated dynamics, we need to derive an arithmetical approach of the filtering process. The transfer function $H_2(P)$ derived in eq. (8) is clearly insufficient to describe the experimental plots. Instead of this a diophantine approach of the filtering process will be presented below.

We now turn to records of frequency fluctuations versus time. These experiments are performed using period counting of the beat frequency f_i over an integration time τ. The low frequency beat signal opens a gate of the reciprocal counter at one of its zero crossings. The register counts the period of both the high frequency counter clock signal and the beat signal. The sampling duration τ determines the integral number of cycles of the counter oscillator accumulated before the gate closes. The number of cycles of the beat signal accumulated during this time interval is finally divided by τ to yield the average frequency $f_i(\tau)$. The average beat frequency being continuously monitored, the dead time, that is the time elapsed between the end of one recording of f_i and the beginning of the next, is zero. By this way the outcome is a collection of $f_i^{(l)}(\tau)$ where l stands for the l^{th} measurement of the averaged beat frequency $f_i(\tau)$. The type of frequency noise being present may be characterized by introducing the Allan deviation which is defined as the mean squared value of the relative frequency deviation between adjacent samples of length τ . Using $y^{(l)}(\tau) = \frac{f_i^{(l)}(\tau)}{f_i}$ it may be rewritten as [7], [8]:

$$\sigma_y^2(\tau) = \frac{1}{2}\langle (y^{(l+1)}(\tau) - y^{(l)}(\tau))^2 \rangle \tag{15}$$

where $l = (1, 2..N)$ stands for the N measurements and $\langle\ \rangle$ means the averaging. This method is widely used to characterize the frequency stability of a test oscillator of frequency $f_o(t)$ against a highly stable reference oscillator of constant frequency f_1 .Using $f_i = f_0(t) - f_1$ at the fundamental mode, we get a relative frequency stability defined as $\frac{\delta f_0}{f_0} = \frac{\delta f_i}{f_i}.\frac{f_i}{f_0} \sim \sigma_y(\tau)$, and the sensitivity f_o/f_i of the frequency measurement set-up may be choosen very large. In the subsequent measurements it is shown that the frequency stability of the test oscillator (the frequency synthesizer) is of the order 10^{-11}.

The graph of the Allan variance versus the sampling time generally obeys power laws τ^{-m} (m integer) over a restricted range of time scales. A dual measure of frequency noise is the power law which is followed by the power spectral density of frequency fluctuations $S_y(f) = f^p$ (p integer). In the hypothesis of stationarity, the time and frequency domains are related with a simple law $m = p + 1$ $(if\ \ -3 < p \leq 1)$ and $m = 2$ $(if\ p \geq 1)$ [7]. Therefore white frequency noise $p = 0$ leads to the Allan deviation $\sigma_y(\tau) \sim \tau^{-1/2}$ and the flicker noise $p = -1$ leads to a flicker floor $m = 0$ in the Allan deviation. In cases when m is not integer, the frequency and time domains may also be related using the Fourier transform, but with less confidence in their meaning. For the experiments we used a highly stable LO oscillator with frequency $f_1 = 5.0206$ MHz. The beat frequency fluctuations $f_i^{(l)}(\tau)$ and the associated Allan deviation $\sigma_y(\tau)$ observed at the fundamental mode

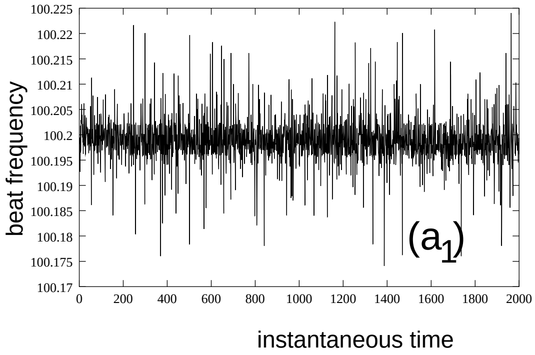

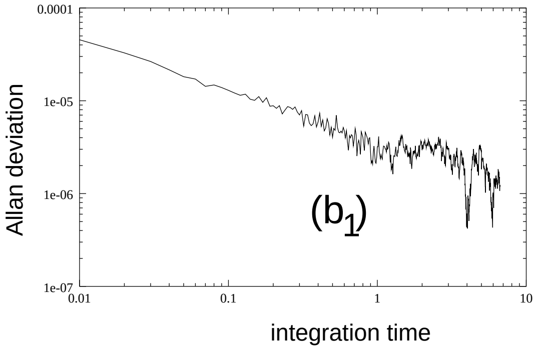

Fig. 3. Instantaneous frequency fluctuations of the beat signal between two input oscillators at $f_1 = 5.0206$ MHz and $f_0 = f_1 + 100$ Hz versus time in units a number of periods (a_1). The corresponding Allan deviation (b_1) corresponds to white frequency noise

$p/q = 1/1$ in three situations. Instantaneous period measurements could be performed in the three cases due to the low frequency of beat signals. The first case $f_i \sim 100\ Hz$ shown in Fig. 3 lies away from the resonance and the corresponding Allan deviation scales as $\sigma_y(\tau) \sim \tau^{-1/2}$ which is typical of white frequency noise. The second case $f_i \sim 4.4\ Hz$ is closer to resonance and the observed Allan deviation Fig. 4 is slowly divergent with scaling law $\sigma_y(\tau) \sim \tau^{1/4}$. Time fluctuations show frequency jumps of magnitude 1 mHz and 2 mHz which are typical of a random telegraph signal (RTS). Finally if the two input oscillators have $f_i \sim 0.5\ Hz$, we found that the RTS converts into a more irregular time dynamics with an approximately constant Allan deviation as shown in Fig. 5, which is typical of a pure $1/f$ noise. Amplitude fluctuations of the beat signals have been recorded in addition to frequency

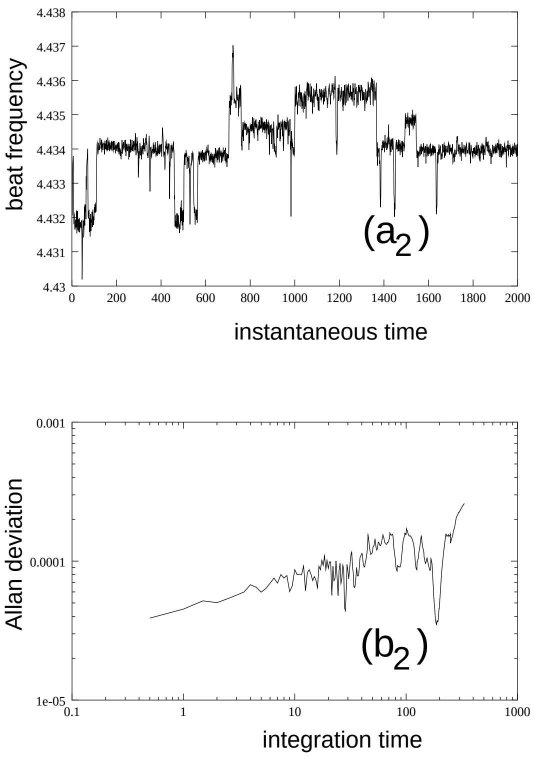

Fig. 4. Instantaneous frequency fluctuations of the beat signal between two input oscillators at $f_1 = 5.0206$ MHz and $f_0 = f_1 + 4.43$ Hz versus time in units a number of periods (a_2). This regime shows a RTS type noise. The corresponding Allan deviation Allan deviation diverges approximately as $\tau^{1/4}$ (b_2)

fluctuations. It has been observed that the conversion from the RTS type signal to the 1/f type signal near the resonance is associated to unpredictible amplitude jumps of the shot noise type. The low frequency amplitude and frequency noises were found recently in bipolar transistors; they were found of 1/f type and correlated to each other [9]. These features will be explained later on the basis of the arithmetical approach.

2 Arithmetic of amplitude-frequency relationships

2.1 The frequency of beat signals from a diophantine approximation

As shown in section 1, the practical operation of the communication receiver always involves many downconverted products at all intermediate frequencies in the bandwidth of the filter. We show that the understanding of the

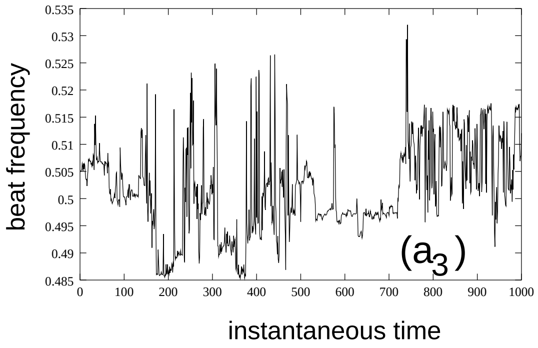

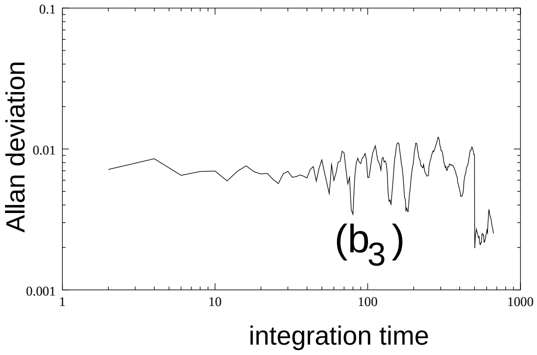

Fig. 5. Instantaneous frequency fluctuations of the beat signal between two input oscillators at $f_1 = 5.0206$ MHz and $f_0 = f_1+0.5$ Hz versus time in units a number of periods (a_3). The corresponding Allan deviation (b_3) corresponds to $1/f$ frequency noise

frequency spectrum of beat signals can be based on number theory and specifically on continued fraction expansions (CFE) of frequency ratios of signals at the input of the mixer. Let $\nu = f_1/f_0$ the LO to RF frequency ratio and $\mu = f_i/f_0$ the IF to RF frequency ratio, the three frequencies operation may be rewritten as:

$$\mu^{(p_i,q_i)} = q_i \mid \nu - \frac{p_i}{q_i} \mid \tag{16}$$

From this form we can guess the device will produce a rational approximation p_i/q_i of the real number ν allowed by the physical constraints, in particular the non linear interaction and the synchronization between the frequencies which take place in the mixer, the properties of the filter, the finite resolution of countings and the unavoidable thermal noise which is present in the set-up. One clearly shows that the approximation is not a decimal one, otherwise we should not understand the hierarchy of interacting basins at intermodulation ratios p_i/q_i. The approximation which is performed is the best one possible accounting for the finite resolution, it is of a diophantine type. Best rational approximations of a real number ν are given from CFE, that is:

$$\nu = a_0 + 1/\{a_1 + 1/\{a_2 + ... + 1/\{a_i + ...\}\}\}; \tag{17}$$

and the a_i's are positive integers (called partial quotients) which are readily obtained from the formulas: $a_0 = [\nu], \alpha_0 = \{\nu\}$ and if $i \geq 1$, $a_i = [1/\alpha_{i-1}], \alpha_i = \{1/\alpha_{i-1}\}$, where $[\nu]$ denotes the integral part of ν and $\{\nu\} = \nu - [\nu]$ is its fractional part. Successive best approximants of ν, that is convergents p_i/q_i are obtained by truncating Eq. (17) at some stage i.

Let us remind the difference between the decimal and the diophantine approximation. From the decimal approximation one builds a series p_i/q_i which verifies the approximation $\left|\nu - \frac{p_i}{q_i}\right| \leq \frac{1}{q_i}$. On the other hand the CFE lead to convergents p_i/q_i which satisfy the far better approximation

$$\left|\nu - \frac{p_i}{q_i}\right| \leq \frac{1}{q_i q_{i+1}} \leq \frac{1}{a_{i+1} q_i^2}. \tag{18}$$

The approximation constant $C(\nu) = lim_{i\rightarrow\infty} q_i^2 \left|\nu - \frac{p_i}{q_i}\right|$ is known as the Markoff constant [10]. It can be shown that the worst numbers (in terms of the diophantine approximation) are $\nu = (\sqrt{5} - 1)/2$, $\nu = \sqrt{2} - 1$, $\nu = (\sqrt{221} - 11)/10$,... They have periodic CFE which are given respectively by $\nu = [0; \bar{1}]$, $\nu = [0; \bar{2}]$, $\nu = [0; \overline{2, 1, 1, 2}]$... corresponding to Markoff constants $C = 1/\sqrt{5}$, $C = 1/(2\sqrt{2})$, $C = 5/\sqrt{221}$...respectively. The symbol $[.; ...]$ means the CFE as in eq.(17) and the bar shows the period of the expansion. They can be predicted by studying the minima of binary quadratic forms. There is also much geometry behind [10].

From (18) one expects that whenever a large partial quotient is reached, the diophantine approximation becomes very efficient and the CFE is truncated at level i. Let us see the effect of restricting CFE at

$$a_i \leq a_{max} \tag{19}$$

Any rational number p_i/q_i has two CFE given by $p_i/q_i = [a_0; a_1, a_2..., a_i]$ and $p_i/q_i = [a_0; a_1, a_2..., a_i - 1, 1]$. Let us consider truncation at a given value a_{max} and numbers ν which are very close to p_i/q_i on the right (resp. on the left); they should be approximated as $p_{i+1}/q_{i+1} = [a_0; a_1, a_2, ...a_i, a_{i+1}]$ (resp.$p_{i+1}/q_{i+1} = [a_0; a_1, a_2, ...a_i - 1, 1, a_{i+1}]$ with $a_{i+1} \geq a_{max}$. But as a result of the truncation at a_{max} those numbers will be approximated from the set of two straight lines $\mu = q_i \left|\nu - \frac{p_i}{q_i}\right|$. The last numbers in the basin of p_i/q_i will be at $\nu_R = [a_0; a_1, a_2, ...a_i, a_{max}]$ and $\nu_L = [a_0; a_1, a_2, ...a_i - 1, 1, a_{max}]$ given by the formulas:

$$\left|\nu_R - \frac{p_i}{q_i}\right| = \frac{1}{q_i q_{i+1}} \; and \; \left|\nu_L - \frac{p_i}{q_i}\right| = \frac{1}{q_i(q_i a_{max} + q_i - q_{i-1})} \tag{20}$$

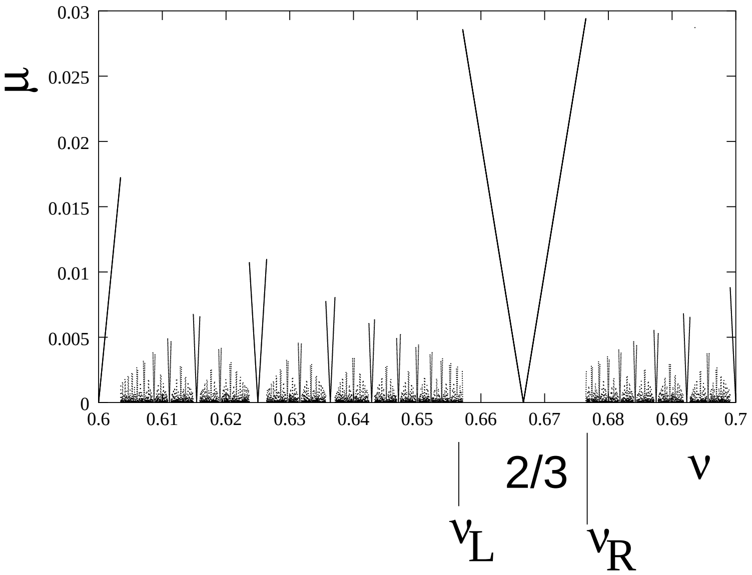

Fig. 6. The intermodulation spectrum resulting from the truncation at $a_{max} = 10$ in the continued fraction expansion of ν. The larger basin in the window $0.6 < \nu < 0.7$ is at the rational $p_i/q_i = 2/3 = [0; 1, 2]$ with $\nu_R = [0; 1, 2, 10] = 21/31$ and $\nu_L = [0; 1, 1, 1, 10] = 21/32$

It is seen that a significant asymmetry results in most cases. Fig. 6 illustrates the result obtained by taking $a_{max} = 10$ and the window $0.6 < \nu < 0.7$. In order to check the validity of the above arithmetical approach we registered the intermodulation spectrum for the device in Fig. 1, using a constant frequency RF signal and a variable frequency LO signal. Acquisition of data was performed using a digital counter with an integration time $\tau_0 = 0.1\ s$. Results are shown in Fig. 7(a). A good fit of the data is obtained accounting for the physical device: products with p_i or q_i even were strongly rejected due to the doubly balanced phase bridge structure of the diode mixer. The theoretical curve is shown in Fig. 7(b). The filtering rate was found to govern the truncation level of CFE in the loop. Using more selective filters at 58 kHz(resp. $3kHz$) we found truncations at values $a_{max} = 9$(resp. 65) also allowing a good fit of the experimental curves.

We just saw the intermodulation spectrum is described from CFE and a resolution increasing with the degree of filtering. It may also be convenient to represent the error μ versus ν on a tree with the number of leaves given from a Farey criterion

$$q_i \leq q_{max}. \tag{21}$$

The Farey series $F_{q_{max}}$ of order q_{max} is defined as the set of irreductible fractions p_i/q_i between 0/1 and 1/1 whose denominators do not exceed q_{max}.

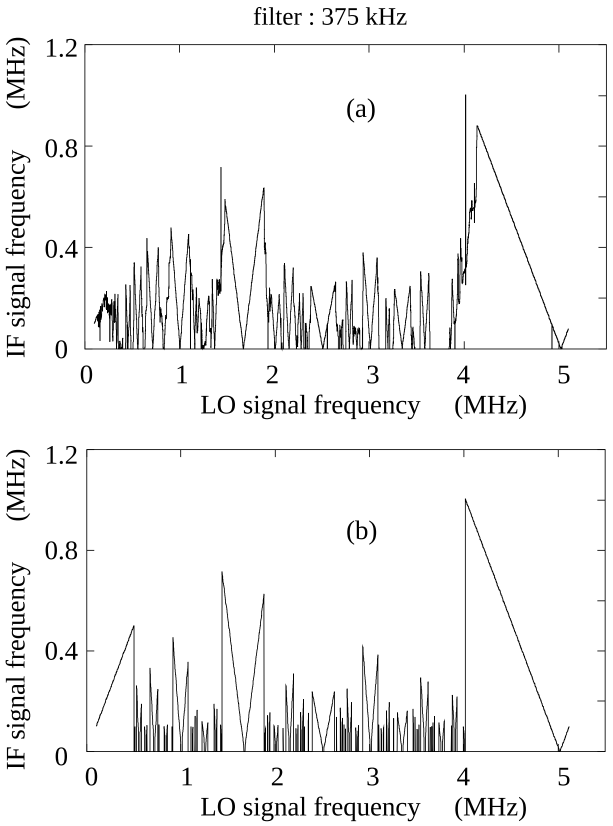

Fig. 7. (a) The intermodulation spectrum for the loop in Fig. 1 and cut-off frequency $f_c = 375kHz$ and the RF constant frequency $f_0 = 5.0206MHz$. (b) The theoretical spectrum. For the fit we chose $a_{max} = 3$ for the fundamental mode $1/1$, $a_{max} = 2$ for products p_i/q_i with p_i and q_i odd and $a_{max} = 20$ for products with p_i or q_i even

Thus F_5 is $\{0/1, 1/5, 1/4, 1/3, 2/5, 1/2, 3/5, 2/3, 3/4, 4/5, 1/1\}$. Between two leaves ending on the real axis at p/q and p'/q' there is one at $(p+p')/(q+q')$ provided q, q' and $q + q'$ do not exceed q_{max}. It arises at the node $\nu = (p + p')/(q + q'), \mu = 1/(q + q')$ as shown in Fig. 8. The number of fractions up to q_{max} is as follows

$$n(q_{max}) = \sum_{k=1}^{q_{max}} \phi(k) = \frac{3\ q_{max}^2}{\pi^2} + 0(q_{max} log(q_{max})) \tag{22}$$

where $\phi(k)$ is the Euler function [5]. Such fractions are called well resolved and n^{-1} is called the resolution. In contrast to criterion (21) a badly resolved experiment is governed by the truncation trick (19) or by truncating CFE at

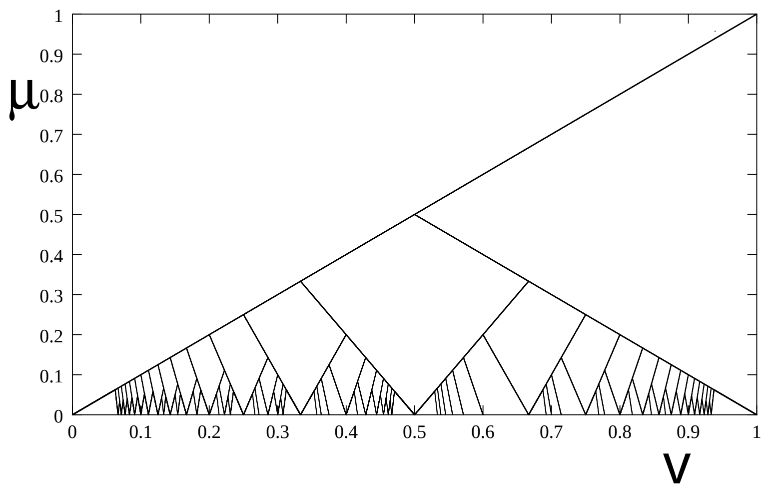

Fig. 8. The increased resolution spectrum as calculated from finite continued fraction expansions of ν from $i_{max} = 1$ to $i_{max} = 3$

a given height:

$$i \leq i_{max}. \tag{23}$$

We will show below their effect in producing $1/f$ type noises.

2.2 The amplitude of beat signals and the Franel-Landau shift

As shown in sect. (2.1) the frequency of beat signals in the demodulator may be interpreted from the diophantine approximation of frequency ratios ν of signals at the input of the mixer. Although this definition accounts for the Farey structure of the underlying tree, it is local and linear: that is nearby frequencies lie on a straight line defined from the truncated CFE of ν; nonlinearity only happens from jumps whenever a partial quotient a_i has been added or removed so that the approximation of ν is controled from a new leave of the tree. Linearity is ensured provided the device operates on a prescribed subharmonic p_i/q_i; this is precisely the property one needs if one uses the demodulator to compare a test oscillator against a reference one.

In contrast to the frequency, the amplitude of beat signals is non linear as shown in Fig. 2b : thus the beat signal is resonant at the subharmonic p_i/q_i, leading to a strong sensitivity of the demodulator to amplitude modulations (AM). It is thus very critical to understand the amplitude of beat signals.

The amplitude $a^{(p_i,q_i)}$ of the beat signal at the subharmonic p_i/q_i can still be defined from number theory. This is achieved by comparing the position of fraction p_i/q_i with respect to the point i/n of the equally spaced scale with n given in eq. (22). The shift is given from:

$$\delta_i = \left| \frac{i}{n} - \frac{p_i}{q_i} \right| \tag{24}$$

and the corresponding amplitude $a^{(p_i,q_i)} = A\ \delta_i$ where A (in Volts) is a reference voltage depending on the sensitivity of the set-up. The shift δ_i was introduced in 1924 by Franel and Landau in the context of a conjecture equivalent to Riemann's hypothesis [5], [11]. The hypothesis relies on the position of zeros of the function $\zeta(s)$ which was introduced by Riemann in 1859 on his celebrated paper on prime numbers. According to Riemann's hypothesis there are an infinite number of non trivial zeros all located on the axis $s = 1/2$. The conjecture will be set forth in section (2.4).

Fig. 9 (curve(1)) shows a plot of the shift δ_i versus $i(i = 1, n(q_{max}))$ for $q_{max} = 150$ (and $n(150) \sim \frac{3}{\pi^2} q_{max}^2 = 6839$) as predicted from (22). An efficient MAPLE procedure was implemented in order to compute Farey fractions and the associated shifts. A computing time increasing like n^2 (30 s for $q_{max} = 100$) was obtained. It can be compared to the experimental plot in Fig. 2a, if we account for the rejection of even intermodulation products due to the balanced structure of the mixer.

As already mentioned in section (1) and will be further extended in our study of frequency fluctuations in section (2.3) our ability to fit the experimental curves depends on our ability to perturb the above result to account for the lack of resolution in the CFE by truncating it at a selected partial quotient a_{max} or at a given height i_{max}. To our knowledge no systematic theory of finite CFE has been developed until know. See [12] for preliminary results and the companion paper by J. Cresson. Here we mention some analytical calculations of Franel-Landau shifts for CFE of low height i_{max} from 1 to 3.

At first order $i_{max} = 1$ the RF to LO frequency ratio is $\nu = 1/a_1, a_1 \leq n^{(1)}(q_{max}) = q_{max}$ so that the shift is as follows:

$$\delta^{(1)}(q_{max}) = \left| \frac{q_{max} - a_1 + 1}{q_{max}} - \frac{1}{a_1} \right| \tag{25}$$

At second order $i_{max} = 2$, $\nu = a_2/(1+a_1a_2)$ with a_1 taking all values between a_1 and $q_{max}-1$ that is $a_1 = (1, q_{max}-1)$ and $a_2 = (1, \left[\frac{q_{max}-1}{a_1}\right])$. The number of ill resolved fractions is

$$n^{(2)}(q_{max}) = 1 + \sum_{a_1=1}^{q_{max}-1} \left[\frac{q_{max}-1}{a_1} \right], \tag{26}$$

with the shift as

$$\delta^{(2)}(q_{max}) = \left| \frac{a_2 + \sum_{k=a_1+1}^{q_{max}-1} \left[\frac{q_{max}-1}{k}\right]}{n^{(2)}(q_{max})} - \frac{a_2}{1+a_1a_2} \right|. \tag{27}$$

The calculation is still more complicated at order $i_{max} = 3$. In such a case we get

$$n_3(q_{max}) = q_{max} + \sum_{a_1=1}^{\left[\frac{q_{max}-1}{2}\right]} \sum_{a_2=1}^{\frac{q_{max}-a_1-1}{a_1}} \left[\frac{q_{max}-a_1}{1+a_1a_2}\right]. \tag{28}$$

There are one term fractions $p_3/q_3 = 1/a_1$ which are located at

$$i = q_{max} - a_1 + 1 \ \text{ if } \ a_1 = (\left[\frac{q_{max}-1}{2}\right], q_{max}), \tag{29}$$

or at the position

$$i = n^{(3)}(q_{max}) - a_1 + 1 - \sum_{k=1}^{k=a_1-1} \sum_{l=1}^{\left[\frac{q_{max}-1-k}{k}\right]} \left[\frac{q_{max}-k}{1+kl}\right] \ \text{ if } \ a_1 = (1, \left[\frac{q_{max}-1}{2}\right]), \tag{30}$$

and there are fractions with three terms $\frac{p_3}{q_3} = \frac{1+a_2a_3}{a_1+a_3+a_1a_2a_3}$ which are located at the position

$$i = n^{(3)}(q_{max}) - (a_1+a_3) - \sum_{l=1}^{a_2} \left[\frac{q_{max}-a_1}{1+a_1 l}\right] - \sum_{k=1}^{a_1} \sum_{l=1}^{\left[\frac{q_{max}-1-k}{k}\right]} \left[\frac{q_{max}-k}{1+kl}\right], \tag{31}$$

with the following range of values

$$a_1 = (1, \left[\frac{q_{max}-1}{2}\right]), \quad a_2 = (1, \left[\frac{q_{max}-1-a_1}{a_1}\right]) \ \text{ and } \ a_3 = (1, \left[\frac{q_{max}-1}{1+a_1a_2}\right]). \tag{32}$$

From these relations, the third order shift may be calculated as:

$$\delta^{(3)}(q_{max}) = \left|\frac{i}{n^{(3)}(q_{max})} - \frac{p_3}{q_3}\right| \tag{33}$$

Since the effective resolution is given from eq.(18) it may be more useful to consider finite length fractions with partial quotient bounded as $a_i \leq a_{max}$. In such a case calculations are easier. At first order $i_{max} = 1$,the number of fractions is $n^{(1)} = a_{max}$ and such fractions $p_1/q_1 = 1/a_1$ are located at

$$i = a_{max} - a_1 + 1 \tag{34}$$

as above in eq.(25). At second order, $n^{(2)} = a_{max}^2$ and fractions $p_2/q_2 = a_2/(1 + a_1a_2)$ are located at

$$i = a_{max}^2 - a_1^2 + a_2 \tag{35}$$

Then for $i_{max}=3$,$n^{(3)}=a_{max}^3+a_{max}$, there are fractions $1/a_1$ located at

$$i=(a_{max}-a_1+1)(a_{max}^2+1) \tag{36}$$

and there are fractions $p_3/q_3=(1+a_2a_3)/(a_1+a_3+a_1a_2a_3)$ that we find at

$$i=(a_{max}-a_1)(a_{max}^2+1)+a_2a_{max}-a_3+1 \tag{37}$$

These explicit calculations are of restricted interest however since they can-

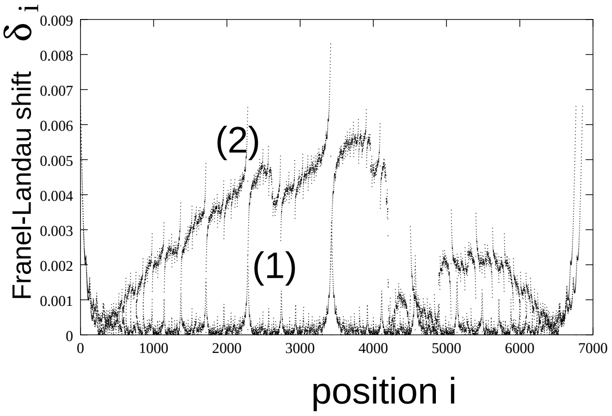

Fig. 9. The Franel-Landau shift δ_i in the well resolved case (curve 1) and for finite length fractions $i_{max}=7$ (curve 2)

not be generalized easily to arbitrary i_{max} or a_{max}. Our MAPLE procedure does not show this drawback (see Fig. 9, curve (2)) and the related comments.

2.3 Diophantine signal processing and 1/f frequency fluctuations

Experiments above clearly demonstrated the diophantine nature of signal processing realized in the receiver shown in Fig. 1. The spectrum of frequencies and amplitudes of beat signals was interpreted in terms of simple rules (16) and (24) of the diophantine type. Although the amplitude-frequency relationship looks very complicated, the dynamics is predictable provided we know what limits the continued fraction expansion (17) of the frequency ratio ν.

One supplementary task is to understand the time dynamics and the origin of the transition from white frequency noise to $1/f$ frequency noise close to resonance. This may be approached from the diophantine nature of "waves"

$$\epsilon_i=\cos\{2\pi\ \ p_i/q_i\}\quad \text{, i=1..n} \tag{38}$$

which constitutes the observed signal, with $n \sim 3\ \ q_{max}^2/\pi^2$ for a well resolved signal, or less if the signal lacks resolution close to resonance. For a continuous (i.e. non diophantine) signal we would expect that the resolution $d\nu = 1/n$ vanishes when n increases, so that by integrating over the frequencies $\nu = p_i/q_i$ we would get the mean value

$$\sigma = \int_{\nu=0}^{\nu=1} \epsilon(\nu) d\nu = \int_{\nu=0}^{\nu=1} \cos(2\pi\nu) d\nu = \sin(2\pi\nu)/2\pi = 0 \tag{39}$$

Such a result is not observed in a finite resolution experiment. Let us consider the discrete partial sum over the waves as:

$$M(i) = \sum_{k=1}^{i} \cos\{2\pi \quad p_k/q_k\} \quad \text{, i=1..n} \tag{40}$$

and the discrete partial sum over the frequency shifts as:

$$S(i) = \sum_{k=1}^{i} |k/n - p_k/q_k| \quad \text{, i=1..n} \tag{41}$$

The terms ϵ_i and δ_i will be called Littlewood term and Franel-Landau shift respectively, and $M(n)$ and $S(n)$ will be called Littlewood and Franel-Landau sums. This refer to the history of Riemann zeta function that we will remind below. Let us first consider the (resonant) case when continued fraction expansions are restricted to a finite partial quotient $a_i \leq a_{max}$. Fig. 10 illustrates the case $a_{max} = 8$. It can be observed in (a) and (b) that the shift δ_i and the wave ϵ_i are fractal like. This is confirmed by computing numerically the fractal dimension (see the companion paper by C. Eckert). Also the mean deviation follow the laws $a_{max}\sigma_F = S(n)a_{max}/n \sim 0.40$ and $a_{max}\sigma_L = M(n)a_{max}/n \sim -1.5$ where n is the number of resolved fractions. It reflects the fact that rationals p_i/q_i are rare beyond the real numbers. We say that this dependence is of the $1/f$ type, since the deviation is constant at all scales n. This is similar to what was obtained in Fig. 5 in the almost resonant interaction of the two input oscillators. Going far away from the resonance we expect to reach a well resolved zone, i.e. at arbitrarily small resolution we should recover the continuous case (39). We found numerically that the deviation scales approximatively as $\sigma_F \sim n^{-3/4}$; this is what we expect also from Riemann hypothesis as will be reminded below. The experiments showed an Allan deviation depending on the integration time as $\sigma \sim \tau^{-1/2}$ (see Fig. 5).

Finally in the intermediate zone, at the outer edge of a resonant zone, there is an increase of the number of fractions and then a decrease of the resolution as shown in Fig. 8. As a result there is an increasing shift δ_i at most subharmonics (Fig. 9, curve(2) where $i_{max} = 7$) as compared to the well resolved case (curve (1)). There we calculate a drift $\sigma_F \sim n^{\alpha}$, with $\alpha > 0$

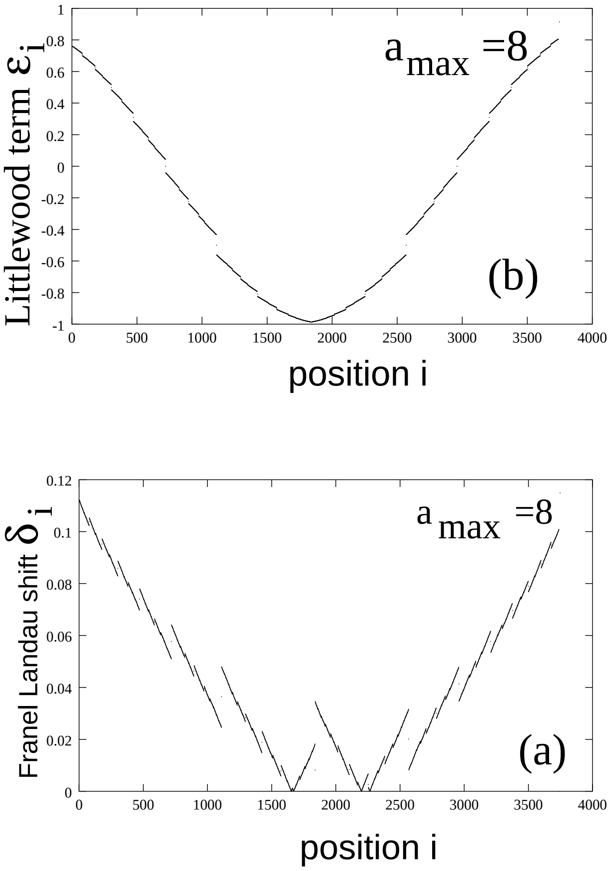

Fig. 10. The Littlewood term (b) and the Franel-Landau shift (a) for fractions with bounded partial quotient a_{max}

depending on the value of i_{max}. For $i_{max} \leq 3$ as calculated above, $\alpha \sim 1/4$ at large n, which looks like the experimental value $\sigma \sim \tau^{1/4}$ in Fig. 5. A similar dependance is obtained for σ_L.

We have given a diophantine approach of the low frequency noise close to a resonance in the receiver. It would be nice at this stage to compare quantitative results given from the Allan deviation $\sigma_y(\tau)$ in (15) and the mathematical result from σ_F or σ_L. To achieve such a goal we need to know precisely what determines the resolution n^{-1} and the truncation at a_{max} or i_{max} and relates these measures to physical parameters, in particular the filter bandwith and the noise of input oscillators.

2.4 The Riemann zeta function and the Riemann hypothesis and physics

In his celebrated paper on the number of prime numbers $\pi(q_{max})$ less or equal than q_{max}, Riemann studies the extension of the zeta function

$$\zeta(s) = \sum_{n=1}^{\infty} \frac{1}{n^s} = \prod_{p \ \ prime} \frac{1}{1-p^{-s}} \text{ (with Re(s)> 1)} \tag{42}$$

to the complex plane s [11]. The connection to $\pi(q_{max})$ is through the log of this function and the Euler product formula is one way to express the decomposition of any integer as a product of powers of prime numbers. Riemann extends the formula to the whole complex plane as follows

$$\zeta(s) = \frac{\Pi(-s)}{2i\pi} \int_{+\infty}^{+\infty} \frac{(-x)^s}{e^x - 1} . \frac{dx}{x} \tag{43}$$

where $\Pi(s) = \int_0^\infty e^{-x} x^s dx$ and $s > -1$ is the Euler integral, and $\Pi(s) = s!$ whenever s is a natural number. In eq.(43) the path of integration begins at $+\infty$, moves to the left down the positive real axis, circles the origin in the counterclockwise direction and returns up the positive real axis to $+\infty$. Formula is valid for all s. It is analytic at all points of the complex plane s except for a single pole at $s = 1$, with residue 1. From calculations already performed by Euler for real x one gets a connection to Bernoulli numbers B_n. Using the expansion near $x = 0$ of $x/(e^x - 1) = \sum_{n=0}^{\infty} B_n x^n/n!$, one gets $B_0 = 1$, $B_1 = -1/2$, $B_2 = 1/6$,$B_4 = -1/30$,$B_6 = 1/42$... and $B_{2n+1} = 0$ if $n > 1$ and the formula $\zeta(-n) = (-1)^n B_{n+1}/(n + 1)$. It follows that the zeta function has "trivial" real zeros at $s = -2, -4, -6$.... Also some real zeta functions are obtained easily as $\zeta(0) = -1/2$, $\zeta(-1) = -1/12$, $\zeta(-3) = -1/120$, $\zeta(2) = \pi^2/6$, $\zeta(4) = \pi^4/90$...

Riemann hypothesis asserts that the only non trivial zeros are located on the imaginary axis $s = 1/2$. Billions of zeros are known all on the critical line but until now the hypothesis has not be proved. It was shown by Littlewood in 1912 that a statement equivalent to Riemann hypothesis may be obtained from the Dirichlet series associated to the inverse of the zeta function as

$$\frac{1}{\zeta(s)} = \sum_{n=1}^{\infty} \frac{\mu(n)}{n^s} \text{ (with Re(s)> 1)} \tag{44}$$

where the Möbius function $\mu(n)$ is zero if n is divisible by a square, is 1 if n is a product of an even number of distinct prime factors and is -1 if n is a product of an odd number of distinct prime factors. The inverse zeta function may be extended to the whole complex plane as:

$$\frac{1}{\zeta(s)} = s \int_0^{\infty} \frac{M(x)}{x^{s+1}} dx \tag{45}$$

and $M(x)=\sum_{n=1}^{x}\mu(n)$ the partial sum over the Möbius function. Littlewood proved that Riemann hypothesis is equivalent to the statement

$$M(x)=0(x^{\frac{1}{2}+\epsilon})\text{ whatever }\epsilon \tag{46}$$

There is an interesting history behind that early work which is reported by Edwards [11]. I refer to the conjecture by Mertens: $|M(x)|<x^{1/2}$ which was disproved only in 1984 and the unproved Stieljes statement in 1885: $M(x)=0(x^{1/2})$. A significant step was achieved in 1920 by Franel and Landau by introducing Farey fractions and the shifts δ_i as given in eq. (24). M(x) may be alternatively written as a sum over the waves $M(n)$ as obtained from (40) so that using eq.(22) Littlewood conjecture is $M(n)=0(n^{\frac{1}{4}+\epsilon})$ whatever ϵ. The equivalent Franel-Landau conjecture is the sum over the shifts δ_i and may be similarly written as $S(n)=0(n^{\frac{1}{4}+\epsilon})$ whatever ϵ where $S(n)$ follows from eq.(41).

It is useful at that point to remind that physical interpretations of (46) have been proposed. In 1931, A. Denjoy [11] suggested that since the Möbius function equals plus or minus one with apparent equal probability (which is $3/\pi^2$) it looks similar to flipping a coin with equal chance for heads and tails, so that $M(x)$ looks like a brownian motion [13]. Consequently the Riemann hypothesis would be true with probability one!

More recently it was observed [14] that the Riemann zeta function $\zeta(s)$ has a quantum statistical interpretation. The unique factorization of an integer into primes, $n=\prod_{p=1}^{p_{max}}p^{N_p}$ translates into a unique decomposition of $\log n=\sum_{p=1}^{p_{max}}N_p\log p$, where N_p corresponds to the number of "particles" of energy $\log p$. It follows that the zeta function is the grand canonical partition function of a "Riemann gas" of quantum bosons of energies $\log p$ (because there is no factor of indistinguishability in the expression for the whole energy $\log n$. Similarly $1/\zeta(s)$ was interpreted as a gas of free "ghost" fermions with the same energy $\log p$ (there is a fermionic aspect since $\mu(n)=0$ at a square number n).

The interpretation of frequency variability is thus embedded into the number theoretical concepts attached to $1/\zeta(s)$. One can go a step ahead by looking at the integer n in Eq. (42) as an integration time τ and consider the variable s as a complex time $1/2+\eta+it$, where η is a small real parameter. Using the decomposition $1/\zeta(s)=Z(t)exp[i\theta(t)]$ one easily computes numerically the discrete Fourier transform $S(\omega)=\sum_{t=0}^{\infty}Z(t)exp[i\omega t]$ with the result $|S(\omega)|^2\sim C^{te}$ on the critical line (at $\eta=0$) and $|S(\omega)|^2\sim 1/\omega$ close to it. This shows a transition from white to $1/\omega$ power spectrum of the modulus of $1/\zeta(s)$. Similarly the power spectral density of the phase $\theta(t)$ decreases like ω^{-2} at the critical line and like ω^{-3} close to it. This corresponds to a transition from white to $1/\omega$ frequency noise as observed in our experiments. In addition one predicts peaks in the power spectral density at $\omega_n=C\ log\ q$ with $q=p^l$, l integer and p prime. The first low frequency peaks are found at 2, 3, 2^2, 5, 7, 2^3, 3^2, 11, 13...This may be explained on the basis of the derivative of *log* $\zeta(s)$ [11] or in relation to a quasiclassical approximation of quantum chaotic orbits [15]

Consequently one has a number theoretical model of the transition from white to $1/f$ frequency noise based on the properties of $1/\zeta(s)$ at or close to the critical line $s = 1/2$. The deviation of the beat note with respect to the perfect oscillation should be in the form $1/\zeta(1/2 + \eta + it)$ with η non zero at resonance and η equal to zero away from it. This model has now to be checked in detail by new experiments related to receivers and particularly in the digital domain.

References

1. Klapper J., Frankle J. T. (1972) Phase-Locked and Frequency-Feedback systems. Academic Press, New-York
2. Maas S. A. (1986) Microwave Mixers. Artech House, Norwood
3. Planat M. (1993) Plurifractal Signature in the Study of Resonances of Dynamical Systems. Fractals, 1:727–734
4. Dos Santos S. , Planat M. (1998) Arithmetical Fractals in an Electronic Loop. In: Novak M. N. (Eds.) Fractals and Beyond. World Scientific, Singapore, 297–306
5. Cvitanovic P. (1992) Circle Maps: Irrationally winding. In: Waldschmidt M. , Moussa P. , Luck J. M. , Itzykson C. (Eds.) From Number Theory to Physics. Springer Verlag, Berlin, 631–658
6. Lichtenberg A. J., Lieberman M. A. (1991) Regular and Chaotic Motion. Springer Verlag, Berlin
7. Allan D. W. (1987) Time and Frequency (Time Domain) Characterization, Estimation and Prediction of Precision Clocks and Oscillators. IEEE Trans. Ultrason. Ferroelect. Freq. Contr., 34:647
8. Eckert C., Planat M., Miehé J. A. (1996) Hidden Order in the Frequency Noise of an Electronic Oscillator. Phys. Rev. E, 54:6093
9. Tagaki K., Serikawa S., Doi T., Mukumoto M. (1997) Phase Noise, Amplitude Noise and their Correlation and the Low Frequency Noise Reduction Method in Bipolar Transistors. In: Clays C., Simoen E. (Eds.) Noise in Physical Systems and 1/f Fluctuations. World Scientific, Singapore, 177–180
10. Perrine S. (1996) L'Arithmétique sur une Surface Percée. In: Planat M. (Eds) Oscillators. Annales des Télécommunications, Paris, 7: 407–420
11. Edwards M. H. (1974) Riemann's zeta function. Acad. Press, New-York
12. Korobov N. M. (1997) On Finite Continued Fractions. Communications of the Moscow Mathematical Society, 1302
13. MacDonald D. K. C. (1962) Noise and Fluctuations: an Introduction. John Wiley and Sons, Paris
14. Julia B. L. (1994) Thermodynamic Limit in Number Theory: Riemann-Beurling Gases. Phys. Rev. A, 203: 425
15. Berry M. V. Semiclassical theory of spectral rigidity. Proc R Soc Lond A400:229-251 (1985)